Journal of Solid State Chemistry 185 (2012) 136–142

Contents lists available at SciVerse ScienceDirect

Journal of Solid State Chemistry

journal homepage: www.elsevier.com/locate/jssc

Optical spectroscopy and excited state dynamics of $CaMoO_4:Pr^{3+}$

Enrico Cavalli [a,*], Fabio Angiuli [a], Philippe Boutinaud [b], Rachid Mahiou [c]

[a] Dipartimento di Chimica Generale ed Inorganica, Chimica Analitica, Chimica Fisica, Università di Parma, Parma, Italy
[b] Clermont Université, ENSCCF, Laboratoire des Matériaux Inorganiques, BP10448, F-63000 Clermont-Ferrand, France
[c] CNRS, UMR6002, F-63177 Clermont-Ferrand, France

ARTICLE INFO

Article history:
Received 14 September 2011
Received in revised form
2 November 2011
Accepted 3 November 2011
Available online 12 November 2011

Keywords:
Calcium molybdate
Praseodymium
Luminescence

ABSTRACT

The luminescence properties of $CaMoO_4:Pr^{3+}$ have been investigated in different experimental conditions in order to obtain information on the excitation and de-excitation pathways of this system. The structure of the emission spectrum depends on different factors: excitation conditions, doping level, temperature, etc. In addition, measurements carried out on single crystals and on micro- or nano-crystalline powders obtained by solid state reaction and sol–gel method have revealed that the morphology of the sample, and then the concentration of the lattice defects, strongly influences the excitation mechanism. These effects have been analysed in the light of available models and a general scheme accounting for the experimental observations has been proposed.

1. Introduction

Mixed oxides activated with Pr^{3+} are extensively investigated as materials for photonics [1,2]. Their application perspectives depend on the efficiency of the emission channels and of the excitation modalities. In many closed shell transition metal oxides, Pr^{3+} ions can be excited either directly in the blue ($^3H_4 \rightarrow {}^3P_{0,1,2}$, $^1I_6$ intraconfigurational transitions) or in the UV (interconfigurational $4f^2 \rightarrow 4f^15d^1$ transitions), or indirectly through UV host excitation followed by an energy transfer and/or an intervalence charge transfer (IVCT) process. The fluorescence dynamics of these systems depend not only on the structure of the energy levels of the rare earth ion but also on their relative position with respect to the host fundamental bands [3,4]. The analysis of the optical spectra measured as a function of the temperature and of the excitation wavelength provides an important information in this connection.

In this paper we investigate the spectral properties of $CaMoO_4:Pr^{3+}$. This material was studied long time ago by Reut and Ryskin in the ambit of a systematic on the 'virtual recharge' (i.e. IVCT) mechanism [5] and was investigated more recently by Zhu et al. [6,7] for white light generation. The emission mechanism proposed by Reut and Ryskin implied the formation of Pr^{4+} as a transient species, while Zhu et al. have discussed their experimental results by asserting that the dopant was stably present in the two valence states +3 and +4, without considering the possibility of charge transfer processes. These different points of view evidence that the excited states dynamics of this system has not been sufficiently clarified yet. Their study, on the other hand, has practical motivations. $CaMoO_4$ belongs to the family of the scheelite structured tungstates and molybdates with general formula MXO_4 (M=Ca, Sr, Ba; X=W, Mo), that can be conveniently activated with rare earth ions in order to develop active media for solid state lasers [1], Raman lasers in particular [8], and phosphors technologies [9,10]. In this context the characterisation of Pr^{3+}-doped $CaMoO_4$ is important in order to extend the available information and the device potentialities of this class of materials.

2. Experimental details

2.1. Synthesis

$CaMoO_4$ pure (CMO, melting temperature: 1445 °C) and doped with Pr^{3+} (Pr:CMO) was synthesised in form of single crystals and powders by different methods. Undoped, 0.1% and 0.5% (Pr/Ca nominal ratio) single crystals, denoted as C00, C01 and C05, respectively, were grown from Na_2MoO_4 flux by the method described in Ref. [11]. Powders of Pr:CMO (0.75% concentration) with different grain sizes were synthesised by solid state reaction (SS07 sample) and Pechini sol–gel (SG07 sample) procedures. In the former case, stoichiometric amounts of MoO_3 (Aldrich, 99.5%), $CaCO_3$ (Carlo Erba, 99.5%) and Pr_6O_{11} (Aldrich, 99.9%) were thoroughly mixed in alumina crucible and fired following the sequence 550 °C (12 h), 650 °C (2 h), 750 °C (2 h) and finally at 900 °C (2 h). In the sol–gel route, appropriate amounts of $CaCO_3$ and Pr_6O_{11} were dissolved in HNO_3 3 M at 75 °C under vigorous

* Corresponding author. Fax: +39 0521 905556.
E-mail address: enrico.cavalli@unipr.it (E. Cavalli).

0022-4596/$ - see front matter © 2011 Elsevier Inc. All rights reserved.
doi:10.1016/j.jssc.2011.11.004

stirring. Citric acid with a 2:1 M ratio with respect to the metal ions was then added as a chelating agent. A stoichiometric amount of $(NH_4)_6Mo_7O_{24}$ (Carlo Erba, 99.5%) was dissolved in hot water and then added to the cationic solution together with PEG (20% w/w) as a gelling agent. The resulting solution was dried at 80 °C for 4 h and then at 120 °C for 12 h. The phosphor was finally obtained after successive calcinations at 500 °C for 2 h and 900 °C for 2 h. The samples were characterised by XRD powder diffraction using a Thermo ARL X'tra diffractometer equipped with a Si(Li) Thermo Electron solid state detector with Cu$K\alpha$ radiation. The morphology of the phosphors particles was examined using of a 515 Philips scanning electron microscope (SEM).

2.2. Spectroscopic measurements

The luminescence properties have been measured in different excitation and temperature conditions. The experiments on the powder samples have been carried out at room temperature only by means of a Fluoromax 3 (Jobin-Yvon) spectrofluorimeter. The 10 K emission spectra of the crystals were measured with a spectroscopic system equipped with a 450 W xenon lamp fitted with a 0.25 m Spex monochromator as source, and a 1.26 m Spex monochromator with a RCA C31034 photomultiplier to analyse and detect the output radiation. The crystals were mounted onto the cold finger of a He-cryocooler (Air Products Displex DE-202). The 300–600 K spectra were measured using a Triax 550 monochromator equipped with a nitrogen-cooled CCD camera and a R928 Hamamatsu photomultiplier (Jobin-Yvon Symphony system). The excitation light was selected from a xenon lamp using a Triax 180 monochromator. The crystals were mounted on a home-made copper holder heated by a thermocoax wire connected to a Thermolyne regulator. The temporal decay profiles were measured at room temperature upon dye (480 nm), nitrogen (337 nm) or Nd:YAG (266 nm) laser excitation and displayed by means of a 400 MHz Lecroy digital oscilloscope with 50 Ω input impedance.

3. Results

3.1. Structural considerations, host luminescence and impurity effects

$CaMoO_4$ is tetragonal (space group $I4_1/a$), with $a=b=5.226$ Å and $c=11.430$ Å, $Z=4$ [12]. In this scheelite-type structure (Fig. 1) the isolated MoO_4^{2-} distorted tetrahedra (S_4 real point symmetry) share their vertices with the CaO_8^{14-} dodecahedral units (distorted, S_4 real point symmetry), which are connected one to another through the edges to form zig-zag chains developing along the crystallographic c axis. Pr^{3+} replaces Ca^{2+}, and this substitution requires charge compensation. It is probably achieved in the crystals by the accommodation of Na^+ ions (present in the flux) at the Ca^{2+} sites and by formation of cationic vacancies in the case of the powders. Whatever the case, the charge compensation results in the perturbation of the local crystal fields acting on the optically active ions. This results in a marked inhomogeneous broadening of their absorption and emission features, even at low temperature. The structure, the phase purity and the morphology of the SS07 and SG07 samples were analysed using XRD and SEM techniques (Fig. 2). The XRD pattern evidence the formation of the desired compounds and the absence of unwanted phases. The SEM image reveals that the SS07 sample has a more uniform morphology and larger average particle size than the SG07 one, whose grains have rather irregular shape and size distribution, with the presence of nanometric particles.

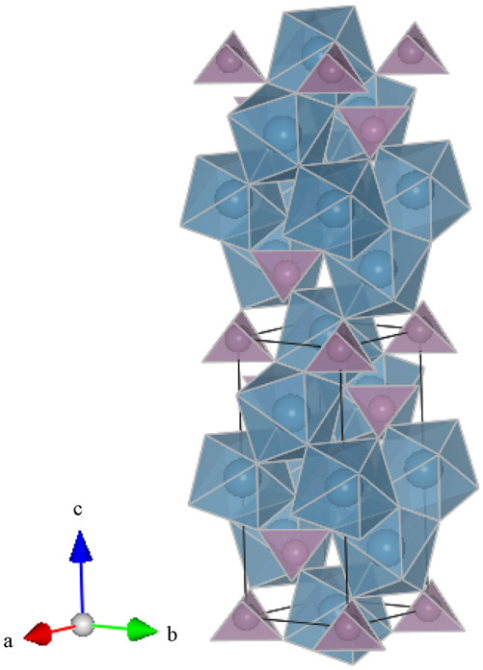

Fig. 1. $CaMoO_4$ structure (elaborated using the VESTA software [13]).

The room temperature excitation and emission spectra of pure CMO (C00 sample) were measured at different emission/excitation wavelengths. They are shown in Fig. 3. The emission band with maximum at 520 nm is assigned to the spin forbidden $^3T_{1,2}\rightarrow{}^1A_1$ transition. The corresponding excitation system is ascribed to the spin allowed $^1T_2\leftarrow{}^1A_1$ charge transfer transition of the regular MoO_4^{2-} unit [14]. The fact that these units are well separated from each other allows inferring that the energy migration is not a favoured process in this system, consistently with the relatively large Stokes shift (about 14000 cm^{-1}) between the excitation and emission maxima. The excitation at around 350 nm reveals an orange component ascribed to charge compensating defects (likely MoO_3) subsequent to the accommodation of aliovalent impurities like Na^+, present in excess in the growth batch [15]. The shoulder occurring at 320 nm in the excitation spectrum has the same origin. The electronic structure and the spectral properties of CMO still constitute an open research topic [16,17] that is beyond the purpose of the present work. It is however clear that the Pr^{3+} incorporation increases the amount of perturbed centres. In addition, it is known that Pr^{3+} can interact with the host giving rise to a photoinduced redox process of the type:

$$Pr^{3+}+Mo^{6+}\rightarrow Pr^{4+}+Mo^{5+}$$

resulting in the formation of the IVCT state. This metal-to-metal charge transfer state can interfere with the fluorescence dynamics of the Pr^{3+} ions, giving rise to various interesting effects [18–20]. The analysis of the IVCT mechanism not only accounts for the experimental observations, but also allows compiling a 'host lattice plus rare earth ion' energy level scheme that can be extended to the whole lanthanide series [4,21]. In the case of CMO this scheme is already available [22] and will be conveniently applied in the present study. As pointed out by some of us [20], the position of the IVCT state is related to the host properties by the empirical equation:

$$IVCT(Pr^{3+},cm^{-1})=58800-49800\frac{\chi_{opt}(M^{n+})}{d(Pr^{3+}-M^{n+})} \quad (1)$$

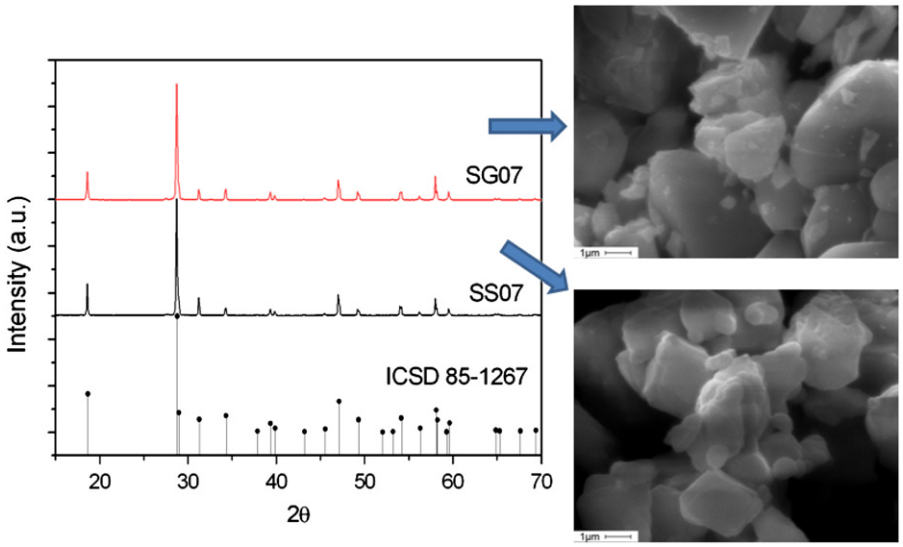

Fig. 2. XRD patterns and SEM images of the SS07 and SG07 samples.

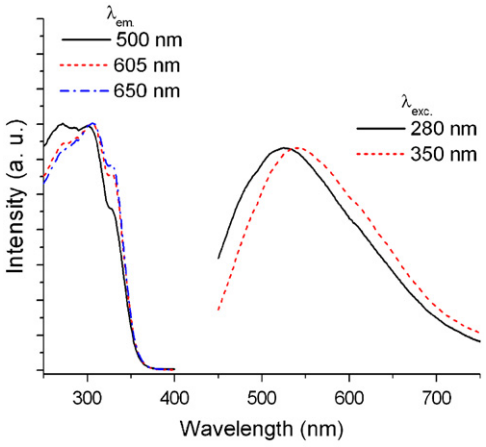

Fig. 3. Room temperature excitation and emission spectra of pure $CaMoO_4$ crystals. The band intensities have been normalised.

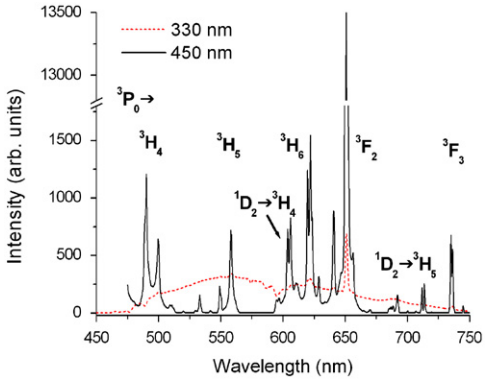

Fig. 4. Low temperature emission spectra of $CaMoO_4:Pr^{3+}$ (C05). Excitation wavelengths: 450 nm (full line) and 330 nm (dotted line).

where $\chi_{opt}(M^{n+})$ is the optical electronegativity of the closed-shell transition metal ion M^{n+} (Mo^{6+} in the present case) and $d(Pr^{3+}–M^{n+})$ is the shortest interatomic distance between Pr^{3+} and M^{n+}. This equation allows estimating the expected energy for the IVCT transition in the investigated material within $\pm 1500\ cm^{-1}$. Its value, about 330 nm, is very close to the excitation edge associated to the perturbed molybdate absorption.

3.2. 10–600 K luminescence spectra and emission dynamics of the Pr^{3+}-doped crystals

The 10 K emission spectra (Fig. 4) of the 0.5% doped crystals (C05) were measured upon excitation at 450 nm in correspondence of the $^3P_2 \leftarrow {}^3H_4$ absorption transition of Pr^{3+} and at 330 nm in correspondence of the host absorption edge and of the $Pr^{3+}(4f^2)Mo^{6+}(5d^0) \rightarrow Pr^{4+}(4f^1)Mo^{5+}(5d^1)$ IVCT transition. In the former case the spectrum consists of manifolds originating from the $^3P_0$ level, with the exception of two multiplets centred at 603 and at 690 nm that are assigned to transitions from the $^1D_2$ state. The observed features are inhomogeneously broadened (FWHM ranging from 40 to 100 cm^{-1}) in consequence of the local disorder around the active ions. The intensity of the $^3P_0 \rightarrow {}^3F_2$ hypersensitive transition at 650 nm is high and compatible with a large value of the Ω_2 Judd–Ofelt parameter, in analogy with the $CaMoO_4:Dy^{3+}$ case [11]. Only the most intense Pr^{3+} features are observable in the 330 nm excited spectrum, in which they are superimposed to the broad host emission. The dips observed in the 480 and 580 nm regions indicate radiative re-absorption from Pr^{3+}.

The room temperature emission spectra of the C01 and C05 crystals measured upon 450 nm excitation are presented in Fig. 5. We note that the intensity ratio $R(^1D_2/^3P_0)$ between the $^1D_2$ and $^3P_0$ emission components decreases as the Pr^{3+} concentration is raised and increases as temperature grows up. These effects result from the de-excitation of the $^3P_0$ state by $^3P_0 \rightarrow {}^1D_2$ multiphonon relaxation and by cross relaxation processes of the type:

$$[^3P_0, {}^3H_4] \rightarrow [^1G_4, {}^1G_4]$$

and

$$[^3P_0, {}^3H_4] \rightarrow [^1D_2, {}^3H_6]$$

that are not resonant (the former in particular) and then favoured by phonon assistance [23]. The cross relaxation involving the $^1D_2$ state:

$$[^1D_2, {}^3H_4] \rightarrow [^1G_4, {}^3F_4]$$

is in practice resonant, so that strong concentration and weak temperature dependences are expected for this process. These mechanisms are schematized in Fig. 6, the excitation process being denoted as the process (1). The excitation spectrum in Fig. 5 is composed of two bands systems: the most intense, in the 420–500 nm range, is assigned to the transitions from the $^3H_4$ ground state to the $^3P_J (J=0, 1, 2)$ and $^1I_6$ levels of Pr^{3+}. The second weaker system, located in the UV region, consists of a broad band ascribed to the host. The superimposition of the host and Pr^{3+} emission signals in the visible region makes it difficult to assess the nature and the effects of the interactions between the host lattice and the optically active dopants. To clarify the situation, we show in Fig. 7 the emission spectra measured upon different excitation wavelengths in the 280–340 nm range. The spectra are composed of the Pr^{3+} emission manifolds overlapping the broad host luminescence. Dips are also present on the high energy side of the host emission, indicating radiative Pr^{3+} re-absorption. In the case of the C01 crystals (Fig. 7(a)), the most intense spectra are those measured upon excitation at 300 and 320 nm. In general, the intensity ratio between the Pr^{3+} and host emissions increases as the excitation wavelength increases, whereas the relative depth of the re-absorption features increases as the excitation wavelength decreases. This indicates that different mechanisms are involved in the excitation of the Pr^{3+} emission.

The 280–300 nm radiation absorbed by the bulk, i. e. by the 'regular' molybdate units, induces the formation of self trapped excitons (STEs), that can decay either radiatively giving rise to the broadband emission centred at 520 nm or non-radiatively through internal non-radiative relaxation and/or energy transfer processes. Owing to the lack of interconnection between the molybdate units, the migration of the STEs through the lattice is reduced and the probability of energy transfer to the rare earth centres very small. We therefore infer that the Pr^{3+} emission is

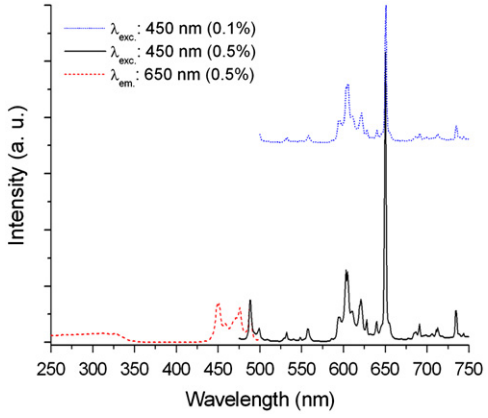

Fig. 5. Room temperature emission spectra of $CaMoO_4:Pr^{3+}$ (C01 and C05 crystals) measured upon Pr^{3+} excitation. Excitation spectrum of the 650 nm emission of C05.

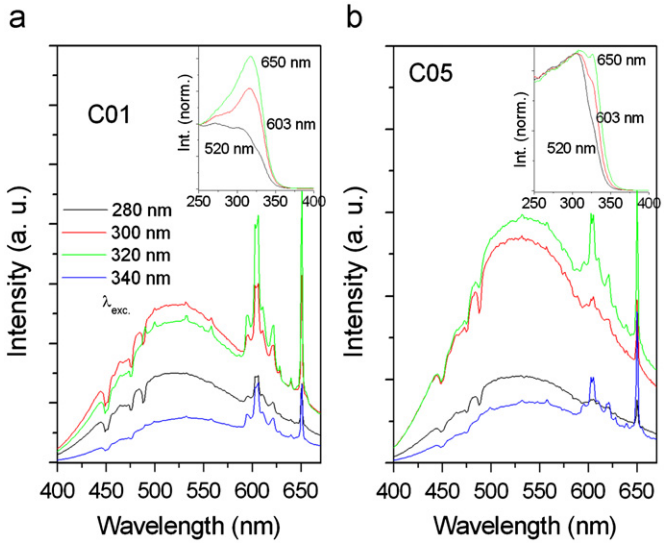

Fig. 7. (a) 298 K emission spectra of the C01 crystals excited at different wavelengths and (b) and 298 K emission spectra of the C05 crystals excited at different wavelengths.

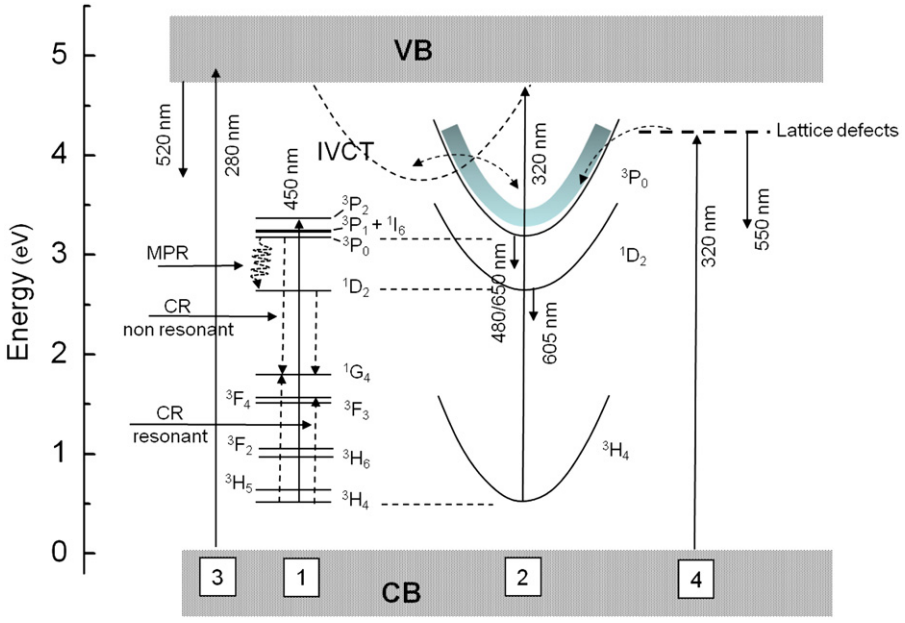

Fig. 6. 'Host lattice + doping ions' energy levels scheme showing the main de-excitation mechanisms following the host excitation. Full arrows indicate emission processes, dotted arrows non-radiative processes.

mostly subsequent to radiative re-absorption of the host emission. Upon excitation in the 320–340 nm range, the dominant processes involve (1) the excitation of the perturbed molybdate centres and their radiative (broadband orange emission) or non-radiative (energy transfer) decays and (2) the population of the IVCT state, thus generating alternative de-excitation pathways. The presence of the IVCT band in the 320 nm region is clearly evidenced in the excitation spectra that are reproduced in the inset of Fig. 7(a). Its intensity progressively grows up as the monitored emission wavelength shifts from 520 nm (regular host emission) to 650 nm (mostly Pr^{3+} $^3P_0 \rightarrow {}^3F_2$ transition). Other evidences of the IVCT effects are also provided by the analysis of the intensity ratio $R(^1D_2/^3P_0)$ vs the excitation wavelength and by investigating the temperature dependence of the Pr^{3+} emission signals up to 600 K. Comparing Figs. 5 and 7(a), it is clear that $R(^1D_2/^3P_0)$ is larger upon excitation at 320 nm than upon excitation at 450 nm. This is explained by the fact that the excitation in the IVCT state is followed by radiationless relaxation to the $^1D_2$ level, by-passing partly the $^3P_0$ level [18]. Despite a general similarity of behaviour, a careful analysis of Fig. 7 allows to evidence that the emission spectra of C05 differ from those of C01 in some aspects concerning: (1) a significant decrease of the intensity ratio between the Pr^{3+} and host emissions, (2) a weaker depth of the re-absorption features, (3) a slight red shift of the host emission maximum and (4) a negligible modification of the excitation spectra upon the monitored emission wavelength (see inset in Fig. 7(b)). We deduce from these observations that increasing the Pr^{3+} doping level in the crystal results in a lower excitation efficiency of the Pr^{3+} ions and/or in a reinforcement of the de-excitation rates operating on the excited Pr^{3+} centres. Concomitantly, the red shift of the host emission suggests an increase of the perturbed molybdate concentration.

Fig. 8 shows the temperature dependence of the emission spectra of C01 and C05 in the range 300–600 K, upon excitation at 337 nm. Similar behaviours are observed for both crystals: the integrated emission from the $^1D_2$ state is nearly constant with the temperature, whereas that from $^3P_0$ is characterised by a plateau in the 300–400 K range, followed by a marked decrease to almost complete quenching at 600 K. These trends are typically observed when the thermal depopulation of the $^3P_0$ state takes place through a cross-over to a Franck–Condon shifted state (IVCT), as observed for Pr^{3+}-doped $CaNb_2O_6$ and $YNbO_4$ [20]. They are rather different from that occurring by mean of multiphonon relaxation and/or cross relaxation mechanisms, as in Pr^{3+}:$KLa(MoO_4)_2$ [3]. We have then reproduced the temperature evolution of the $^3P_0$ emission intensity by means of the Struck and Fonger model [24]:

$$\frac{I}{I_0} = \left[1 + A\exp\left(-\frac{\Delta E}{kT}\right)\right]^{-1} \quad (2)$$

where A is close to 10^7 and ΔE is the activation energy from the emitting state to its crossover with the quenching state. Its value is of about 4100 cm^{-1}, and it is consistent with the relative positions of the parabolas associated to the $^3P_0$ and IVCT states in the single configurational coordinate diagram presented in Fig. 6.

The decay profiles of the host emission were measured at room temperature upon 337 nm excitation as a function of the Pr^{3+} doping level (Fig. 9(a)). They are similar one to another and can be reproduced by means of the sum of two exponential functions yielding decay times of 4 and 19 μs. These values are much shorter than the intrinsic lifetime of the emitting triplet state that is usually of the milliseconds order, and reflect the strong temperature quenching operating on the molybdate emission [15]. In principle these double exponential profiles could be related to the presence of regular and defect molybdate centres. To our knowledge however, the previous literature concerning the $CaMoO_4$ luminescence does not report indications supporting this hypothesis, that we consider a reliable possibility needing further confirmation. The Pr^{3+} decay profiles were measured at 77 and 298 K in C05, upon direct excitation into the ^3P_J (J=0, 1, 2) manifold. The $^3P_0$ emission (Fig. 9(b)) decays as a single exponential with a time constant of the order of 0.6 μs. This short value confirms that different processes contribute to the non-radiative depopulation of this level, as already pointed out. The $^1D_2$ decay curve (Fig. 9(c)) is not single exponential. At 300 K it was reproduced by the Inokuti–Hirayama model for energy transfer in absence of migration [25]:

$$\phi(t) = A\exp\left[-\frac{t}{\tau} - \alpha\left(\frac{t}{\tau}\right)^{3/s}\right] \quad (3)$$

where $\phi(t)$ is the emission intensity after pulsed excitation, A is the intensity of the emission at t=0, τ is the lifetime of the isolated donor and s=6 for dipole–dipole (D–D), 8 for dipole–quadrupole (D–Q) and 10 for quadrupole–quadrupole (Q–Q) interaction. The parameter α provides information on the

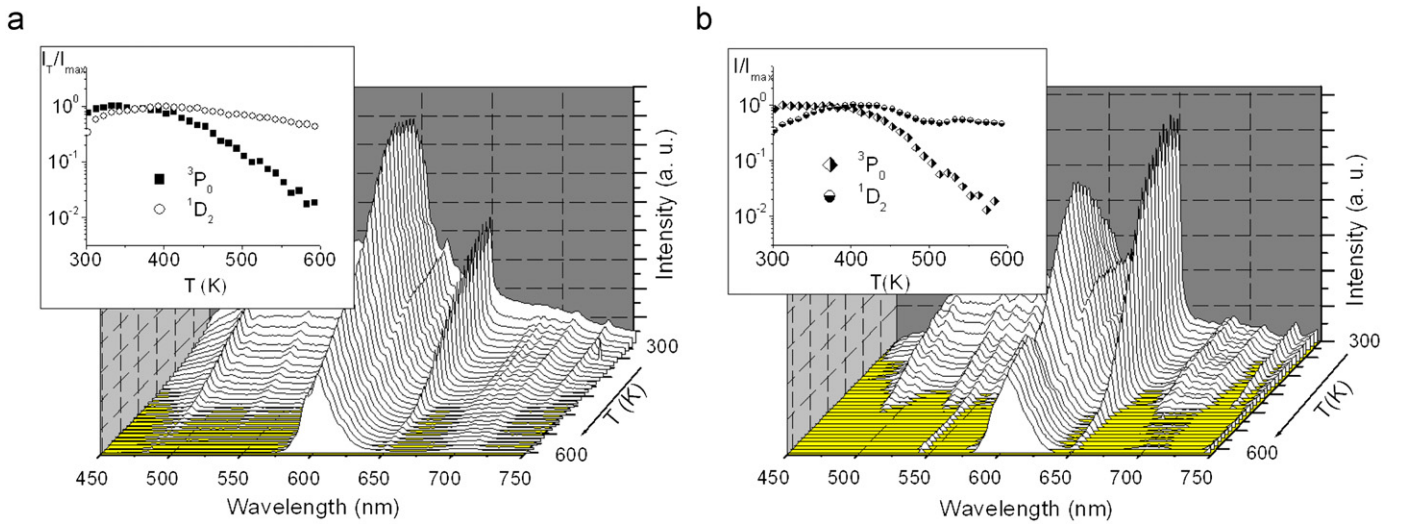

Fig. 8. Emission behaviour in the high temperature regime. (a): CMO:Pr 0.1%, λ_{exc}.: 337 nm and (b) CMO:Pr 0.5%, λ_{exc}: 337 nm. The insets of the figures report the temperature behaviour of the integrated intensities of the $^1D_2$ and $^3P_0$ emissions.

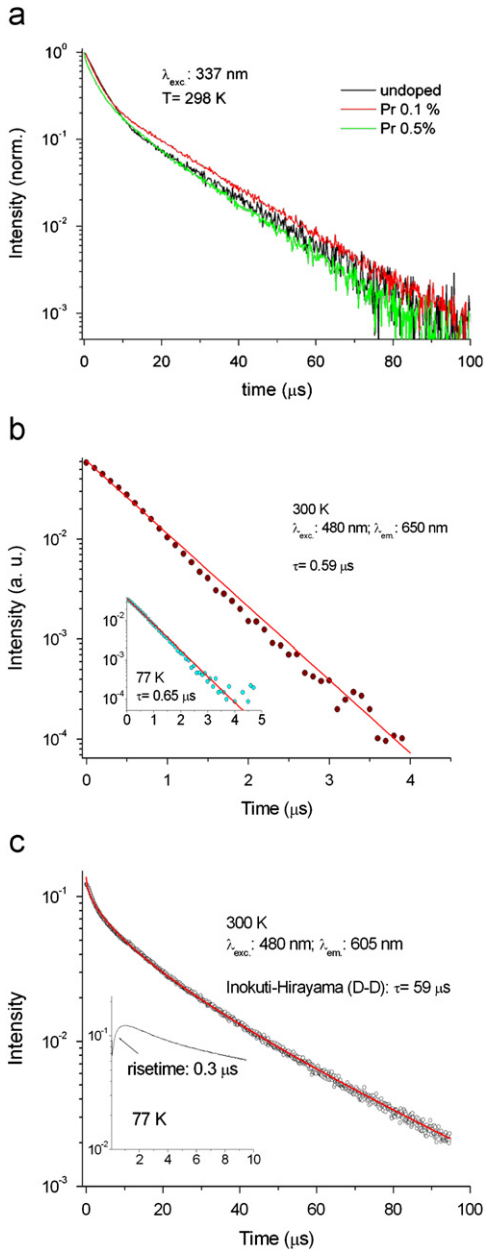

Fig. 9. Emission decay profiles of the broadband emission in pure and Pr^{3+} doped crystals (a) and of the $^1D_2$ (b) and $^3P_0$ emission (c) in CMO:Pr 0.5%.

probability of the energy transfer process:

$$\alpha = \frac{4}{3}\pi\Gamma\left(1-\frac{3}{s}\right)N_a R_0^3 \quad (4)$$

where Γ is the gamma function, N_a the concentration of the acceptor expressed in ions $\cdot$ cm^{-3} and R_0 is the critical distance. We have fitted the decay curves by means of Eq. (3) by considering a D–D process and A, τ and α as adjustable parameters. The obtained τ value is 59 μs and the critical distance for the transfer, evaluated by means of Eq. (4), is of about 16 Å, consistent with the statistically estimated mean shortest distance between the doping ions in the lattice (15.5 Å). The mechanism responsible for this behaviour is presumably the abovementioned cross relaxation process. The 77 K decay curve presents a risetime in its initial part, as a result of the feeding process from the upper $^3P_0$ level.

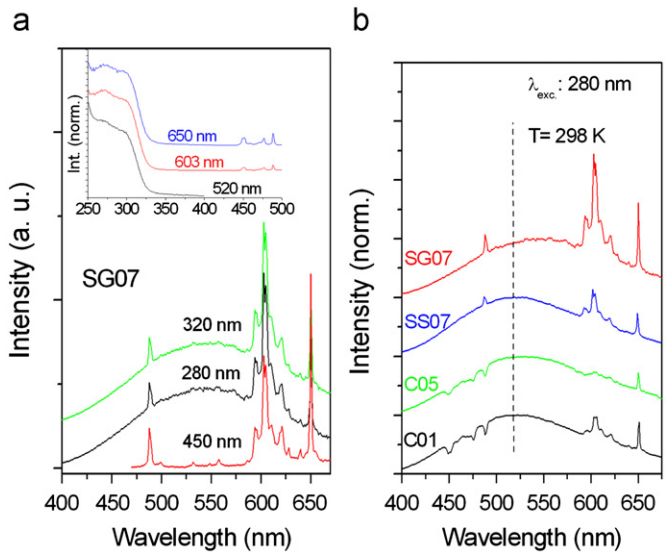

Fig. 10. (a) 298 K emission spectra of the SG07 sample upon different excitation wavelengths. In the inset: excitation spectra measured at different emission wavelengths. (b) comparison between the emission spectra of all samples upon 280 nm excitation. The spectra are normalised with respect to the broadband maximum.

3.3. *Luminescence spectra of the Pr^{3+}-doped powders*

It is interesting to compare the spectra of the crystals to those of micro-sized polycrystalline SG07 and SS07 samples. These are reported in Fig. 10. We note: (1) the absence of re-absorption effects in the powders, (2) the independence of the structure of the UV excited emission on the excitation wavelength (Fig. 10(a)), (3) the high energy shift of the UV excitation band with respect to the crystals case (Fig. 7) and its independence on the monitored emission wavelength, (4) the much stronger intensity of this band relative to the Pr^{3+} intraionic and IVCT transitions (inset of Fig. 10(a)). This indicates that the Pr^{3+} emission in the powders is mostly governed by host sensitization processes, in agreement with the observations of Zhu et al. [6]. It is also interesting to note the red shift of the broadband emission in the SG07 spectrum compared to the SS07 spectrum (Fig. 10(b)). This is consistent with the more effective role of the defects associated to the wider distribution of the grain morphology and to the presence of nano-sized particles.

4. Discussion

The UV excited luminescence processes of Pr^{3+}:$CaMoO_4$ have been summarily schematized in the diagram sketched in Fig. 6. In the low concentrated crystal (C01), the Pr^{3+} emission is mostly generated upon excitation in the IVCT state (process (2)). This charge transfer state originates from the photoinduced interaction between 'regular' MoO_4^{2-} units and Pr^{3+} ions. Internal relaxation then takes place to feed the $^3P_0$ and $^1D_2$ levels, and the relative population of these two levels depends on the temperature (Fig. 8). Most of the energy absorbed in the 280–300 nm region is relaxed radiatively as a broadband emission (process (3) of Fig. 6). Part of it is reabsorbed to raise the Pr^{3+} emission. As the Pr^{3+} concentration is raised in the crystal (C05), the probability for the STEs to carry their energy to a Pr^{3+} ion is increased and the re-absorption process is less probable (i.e. reduced dips in Fig. 7(b)). The Pr^{3+} emission is however not enhanced compared to C01 crystal because of the concomitant reinforcement of quenching processes (cross-relaxation mostly).

In the powder samples, the density of perturbed molybdates centres is increased with respect to the single crystals, as attested by the broader emission profile (compare Figs. 7 and 10). The spectroscopic data (Fig. 10(b)) evidence that the maximum presence of defects is found in the SG07 case. Curiously, this is the sample in which the Pr^{3+} emission is the stronger upon excitation at 280 nm. In order to account for this behaviour we have to consider that in the powders case the interaction with the excitation light gives rise to scattering processes to a much greater extent than in single crystals and constitutes, as a matter of fact, a superficial phenomenon. In these conditions the direct excitation of the Pr^{3+} ions 'via' intraionic $4f \rightarrow 4f$ or IVCT transitions become less efficient in consequence of the reduced penetration depth of the incident radiation. The remaining excitation process is the host sensitization. Moreover, it has to be pointed out that in the powder samples the nature of the defects is different and the probability of having Pr^{3+} ions located in proximity of perturbed molybdate units is much higher than in the crystals, in consequence of their morphological properties, of their higher doping level and also of their different charge compensation mechanisms, as pointed out in Section 3.1. We suppose, consistently with the behaviour observed in Fig. 10, that the energy transfer process from the defect molybdate centres to the active dopants (described by process (4) of Fig. 6) could be relatively efficient, at variance with that involving the regular MoO_4^{2-} ions. The relative stronger Pr^{3+} emission features in SG07 (constituted in part by nano-sized particles) compared to SS07 is in agreement with this hypothesis, even if it could also be ascribed to a lower efficiency of cross-relaxation processes in the former case. We think in fact that the sol–gel methodology allows a better statistical distribution of the dopants within the host lattice than the solid state reaction procedure. In our opinion, the role played by the defect centres in the sensitization of the Pr^{3+} emission is certainly important but has yet to be fully understood.

5. Concluding considerations

The emission dynamics of the CMO:Pr system have been explored under different experimental conditions. Direct excitation of Pr^{3+} at 450 nm gives rise to a fluorescence spectrum composed of features originating in the $^3P_0$ and $^1D_2$ levels, whose relative intensities depend on intermanifold processes like multiphonon relaxation and cross relaxation processes. In the case of UV excitation the situation is much more complicated, since the experimental results have evidenced that the sample morphology plays an important role in determining the main mechanism involved in the de-excitation pathways. Measurements carried out on samples obtained by different synthetic routes have allowed us to stress the role of the lattice defects, that in the investigated system are optically active. In this connection, we have proposed two different host excitation mechanisms: in the single crystals the UV excitation energy is preferentially transferred to the Pr^{3+} ions from the 'regular' MoO_4^{2-} units through a mechanism involving the IVCT state, whereas in the powder materials the Pr^{3+} emission is mainly excited through the energy transfer from perturbed molybdate centres. This hypothesis is consistent with the experimental data and constitutes, in our opinion, a model that will be conveniently extended to the analysis of the optical properties of a number of analogous materials in order to verify its reliability. We are planning further work in this direction.

References

[1] A.A. Kaminskii, Crystalline Lasers: Physical Processes and Operating Schemes, CRC Press, New York, 1996.
[2] W.M. Yen, Phosphor Handbook, CRC Press, Boca Raton USA, 2000.
[3] E. Cavalli, P. Boutinaud, M. Bettinelli, P. Dorenbos, J. Sol. Stat. Chem. 181 (2008) 1025.
[4] P. Dorenbos, A.H. Krumpel, E. van der Kolk, P. Boutinaud, M. Bettinelli, E. Cavalli, Opt. Mater. 32 (2010) 1681.
[5] E.G. Reut, A.I. Ryskin, Phys. Status Solidi (a) 17 (1973) 47.
[6] F. Zhu, Z. Xiao, F. Zhang, L. Yan, A. Huang, J. Lumin. 131 (2011) 22.
[7] F. Zhu, Z. Xiao, F. Zhang, L. Yan, A. Huang, Appl. Phys. A 101 (2010) 689.
[8] T.T. Basiev, A.A. Sobol, Y.K. Voronko, G.P. Zverev, Opt. Mater. 15 (2000) 205.
[9] J. Liu, H. Lian, C. Shi, Opt. Mater. 29 (2007) 1591.
[10] Z. Zhang, H. Chen, X. Yang, J. Zhao, Mater. Sci. Eng. B 145 (2007) 34.
[11] E. Cavalli, E. Bovero, A. Belletti, J. Phys. Condens. Matter 14 (2002) 5221.
[12] E. Gürmen, E. Daniels, J.S. King, J. Chem. Phys. 55 (1971) 1093.
[13] K. Momma, F. Izumi, J. Appl. Crystallogr. 41 (2008) 653.
[14] Y. Zhang, N.A.W. Holzwarth, R.T. Williams, Phys. Rev. B 57 (1998) 12738.
[15] J.A. Groenink, C. Hakfoort, G. Blasse, Phys. Status Solidi (a) 54 (1979) 477.
[16] M. Fujita, M. Itoh, S. Takagi, T. Shimizu, N. Fujita, Phys. Status Solidi (b) 243 (2006) 1898.
[17] C. Pu, T. Liu, Q. Zhang, Phys. Status Solidi (b) 245 (2008) 1586.
[18] P. Boutinaud, R. Mahiou, E. Cavalli, M. Bettinelli, J. Lumin. 122-123 (2007) 430.
[19] P. Boutinaud, P. Putaj, R. Mahiou, E. Cavalli, A. Speghini, M. Bettinelli, Spectrosc. Lett. 40 (2007) 209.
[20] P. Boutinaud, E. Cavalli, M. Bettinelli, J. Phys. Condens. Matter 19 (2007) 386230.
[21] A. Krumpel, E. van der Kolk, P. Dorenbos, P. Boutinaud, E. Cavalli, M. Bettinelli, Mater. Sci. Eng. B 14 (2008) 114.
[22] E. Cavalli, P. Boutinaud, R. Mahiou, M. Bettinelli, P. Dorenbos, Inorg. Chem. 49 (2010) 4916.
[23] R. Naccache, F. Vetrone, A. Speghini, M. Bettinelli, J.A. Capobianco, J. Phys. Chem. C **112** (2008) 7750.
[24] C.W. Struck, W.H. Fonger, J. Appl. Phys. 42 (1971) 4515.
[25] M. Inokuti, F. Hirayama, J. Chem. Phys. 43 (1965) 1978.